Cross sections of the ^{143}Nd(n,α)^{140}Ce and ^{147}Sm(n,α)^{144}Nd reactions in the MeV neutron energy region

Yu. M. Gledenov,[1] M. V. Sedysheva,[1] V. A. Stolupin,[1] Guohui Zhang,[2,*] Jiaguo Zhang,[2] Hao Wu,[2] Jiaming Liu,[2]
Jinxiang Chen,[2] G. Khuukhenkhuu,[3] P. E. Koehler,[4] and P. J. Szalanski[5]

[1]*Frank Laboratory of Neutron Physics, JINR, Dubna 141980, Russia*
[2]*State Key Laboratory of Nuclear Physics and Technology, Institute of Heavy Ion Physics, Peking University, Beijing 100871,
People's Republic of China*
[3]*Nuclear Research Centre, National University of Mongolia, Ulaanbaatar, Mongolia*
[4]*Physics Division, Oak Ridge National Laboratory, Oak Ridge, Tennessee 37831, USA*
[5]*University of Lodz, Institute of Physics, Lodz, Poland*

Cross sections and forward/backward ratios in the laboratory reference system were measured for the ^{143}Nd(n,α)^{140}Ce reaction at 4.0, 5.0, and 6.0 MeV and for the ^{147}Sm(n,α)^{144}Nd reaction at 5.0 and 6.0 MeV. A twin-gridded ionization chamber and large-area back-to-back ^{143}Nd$_2$O$_3$ samples and ^{147}Sm$_2$O$_3$ samples were employed. Experiments were performed at the 4.5 MV Van de Graaff accelerator of Peking University, China. Fast neutrons were produced through the ^{2}H(d,n)^{3}He reaction by using a deuterium gas target. A small ^{238}U fission chamber was employed for absolute neutron flux determination, and a BF$_3$ long counter was used as the neutron flux monitor. Present experimental data are compared with previous measurements, evaluations, and model calculations.

I. INTRODUCTION

Cross section data for the emission of charged particles following fast neutron bombardment are important in nuclear engineering applications as well as basic nuclear physics. Because Q values for the ^{143}Nd(n,α)^{140}Ce and ^{147}Sm(n,α)^{144}Nd reactions are relatively large (9.722 and 10.13 MeV, respectively), cross sections are measurable even at low energies; hence, measurements and analysis have been made at thermal and resonance energies, as well as for 14 MeV neutrons [1–13].

In the MeV neutron energy region, however, no experimental data exist for the ^{147}Sm(n,α)^{144}Nd reaction, and there is only one datum for the ^{143}Nd(n,α)^{140}Ce reaction at $E_n = 3.0$ MeV with large uncertainty [14]. As a result, there are very large differences among different evaluated nuclear data libraries such as ENDF/B-VII, ENDF/B-VI, JEFF3.1, and JENDL3.3 [15]. For example, at $E_n = 6.0$ MeV, the evaluated cross sections for ^{143}Nd(n,α)^{140}Ce are 0.74, 1.08, 0.12, and 0.34 mb, and those for ^{147}Sm(n,α)^{144}Nd are 0.40, 1.32, 0.17, and 0.13 mb, respectively, in the above-mentioned four data libraries.

To resolve these differences, cross section measurements in the MeV neutron energy region are demanded for the two reactions. Measuring ^{143}Nd(n,α)^{140}Ce and ^{147}Sm(n,α)^{144}Nd cross sections at MeV energies is difficult, because both the cross section and available monoenergetic neutron flux are relatively small, and the backgrounds potentially large. Measurements are further limited by the fact that the samples must be relatively thin to limit systematic uncertainties related to straggling of the outgoing α particles. Therefore, to obtain

sufficient statistics, large area samples, a detector having high efficiency and large solid angle, and long measurement durations are needed.

In the present work, a twin gridded ionization chamber was used as the α-particle detector. The detection efficiency and solid angle of the twin gridded ionization chamber are nearly 100% and 4π, respectively. Back-to-back large-area ^{143}Nd$_2$O$_3$ samples and ^{147}Sm$_2$O$_3$ samples were employed for ^{143}Nd(n,α)^{140}Ce and ^{147}Sm(n,α)^{144}Nd cross section measurements, respectively. Cross sections and forward/backward ratios for the emitted α particles in the laboratory reference system were measured for the ^{143}Nd(n,α)^{140}Ce reaction at 4.0, 5.0, and 6.0 MeV and for the ^{147}Sm(n,α)^{144}Nd reaction at 5.0 and 6.0 MeV. Because (n, charged particle) cross sections generally are lower for higher Z materials, krypton was used instead of the more usual argon as the main working gas in the ionization chamber. Although the background was still relatively strong at lower charged-particle energies, α events from ^{143}Nd(n,α)^{140}Ce and ^{147}Sm(n,α)^{144}Nd reactions could be separated from the background, because Q values of the measured reactions are large compared to those of other reactions.

II. EXPERIMENTS

Experiments were performed at the 4.5 MV Van de Graaff accelerator of Peking University, China. As shown in Fig. 1, the setup of our experiment consisted of three main parts: the twin gridded ionization chamber, neutron source, and neutron flux detectors. The twin gridded ionization chamber, comprised of two symmetric sections with a common cathode, was constructed at the Frank Laboratory of Neutron Physics in Dubna, Russia. The outer wall of the chamber was an

*Corresponding author: guohuizhang@pku.edu.cn
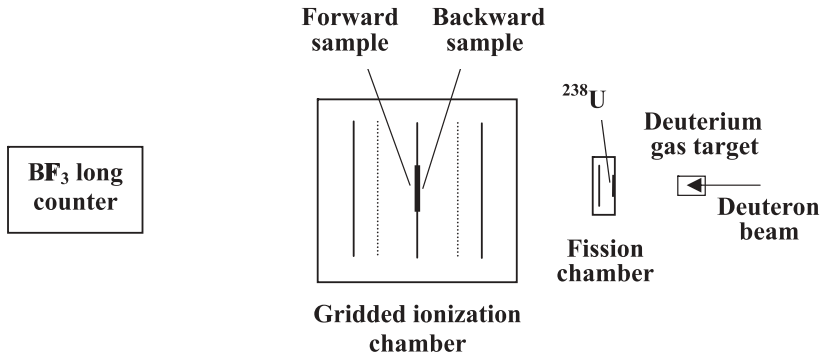
FIG. 1. Setup of the experiment.

aluminum cylinder, 29.0 cm in height by 37.0 cm in diameter, with 2.0 mm thick walls. The cathode, grids, and anodes were rectangular. The grids consisted of parallel tungsten wires, coated with gold, which were 0.10 mm in diameter and spaced 2.0 mm apart. The effective grid area was $16 \times 18 \text{ cm}^2$. Distances from the cathode to grid and from the grid to anode were 75 and 20 mm, respectively.

For the $^{143}\text{Nd}(n,\alpha)^{140}\text{Ce}$ reaction measurement, a mixture of $\text{Kr} + 2.89\% \text{ CO}_2$ was used as the working gas for the ionization chamber. Gas pressure of 1.90 atm was used to ensure α particles from the reaction were stopped before reaching the grids. High voltages for the cathode, grid, and anode were -3000, 0, and 1500 V, respectively, to allow complete collection of the electrons.

For the $^{147}\text{Sm}(n,\alpha)^{144}\text{Nd}$ reaction measurement, $\text{Kr} + 2.27\% \text{ CO}_2$ was used as the working gas. Gas pressure of 2.20 atm was used, and high voltages for the cathode, grid, and anode were -3400, 0, and 1700 V, respectively.

Parameters of the samples are described in Table I. Forward and backward samples were back-to-back set at the common cathode of the gridded ionization chamber for forward α events (0–90°) and backward α events (90–180°) measurement simultaneously. Two retractable α sources inside the gridded ionization chamber were used for energy calibration and adjustment of the data acquisition system. Neutrons were produced through the $^2\text{H}(d,n)^3\text{He}$ reaction by using a deuterium gas target. The diameter and the length of the cylindrical gas cell were 0.9 and 2.0 cm, respectively. The gas cell was separated from the vacuum tube through a molybdenum foil 5.0 μm in thickness. The deuterium gas pressure was 2.9–3.1 atm during the experiment. The energies of the accelerated deuteron beam before reaching the molybdenum foil were 1.79, 2.46, and 3.26 MeV, which according to

Monte Carlo simulations, correspond to neutron energies of 4.0, 5.0, and 6.0 MeV, with energy spreads of 0.23, 0.16, and 0.12 MeV, respectively.

Absolute neutron flux was determined by a small parallel plate ^{238}U fission chamber positioned between the gridded ionization chamber and the gas target. The enrichment of the ^{238}U isotope was better than 99.997%. The mass and diameter of the ^{238}U sample were 547.2 $(1 \pm 1.3\%)$ μg and 2.0 cm, respectively. The working gas of the fission chamber was flowing $\text{Ar} + 3.73\% \text{ CO}_2$ gas at a pressure slightly higher than 1.0 atm. A BF_3 long counter was used as a neutron flux monitor during measurements. The centers of the gridded ionization and fission chambers were at 0°, and the samples were perpendicular to the incident neutron beam. The axis of the BF_3 long counter was also at 0° to the beamline.

For the $^{143}\text{Nd}(n,\alpha)^{140}\text{Ce}$ reaction measurement, the distances from the center of the gas target to the ^{238}U and $^{143}\text{Nd}_2\text{O}_3$ samples were 3.45 and 35.5 cm, respectively. The intensity of the deuteron beam was about 3.5 μA. Durations for $E_n = 4.0$, 5.0, and 6.0 MeV measurements were about 36, 22, and 19 h, respectively.

For the $^{147}\text{Sm}(n,\alpha)^{144}\text{Nd}$ reaction measurement, the distances from the center of the gas target to the ^{238}U and $^{147}\text{Sm}_2\text{O}_3$ samples were 3.40 and 35.0 cm, respectively. The intensity of the deuteron beam was about 2.5 μA, and durations for $E_n = 5.0$ and 6.0 MeV measurements were about 28 and 22 h, respectively.

Two-dimensional cathode versus anode spectra for both forward- and backward-emitted α particles were recorded simultaneously. The block diagram of the electronics can be found in Ref. [16]. Anode spectra of the ^{238}U fission chamber were also recorded at the same time for absolute neutron flux determination.

$^{143}\text{Nd}(n,\alpha)^{140}\text{Ce}$ and $^{147}\text{Sm}(n,\alpha)^{144}\text{Nd}$ cross sections were calculated using the following formula:

$$\sigma_\alpha = K\sigma_f \frac{N_\alpha}{N_f} \frac{N_{238U}}{N_{\text{sample}}}, \tag{1}$$

where σ_α denotes the cross section to be measured; σ_f is the standard $^{238}\text{U}(n,f)$ cross section from the ENDF/B-VII.0 library at the relevant energy; N_α and N_f are numbers of α events from the measured (n,α) reaction and fission events from the $^{238}\text{U}(n,f)$ reaction, respectively; N_{238U} and N_{sample} are the atom numbers of ^{238}U and ^{143}Nd (or ^{147}Sm) in the

TABLE I. Description of samples.

	^{143}Nd samples	^{147}Sm samples
Sample material	$^{143}\text{Nd}_2\text{O}_3$	$^{147}\text{Sm}_2\text{O}_3$
Enrichment of isotope	83.5% ^{143}Nd	95.3% ^{147}Sm
Sample thickness, mg/cm^2	4.077[a], 3.875[b]	5.00[a], 5.00[b]
Sample diameter, cm	10.8[a], 10.8[b]	11.0[a], 11.0[b]
Aluminum backing thickness, mm	0.127	1.0

[a]Forward sample.
[b]Backward sample.
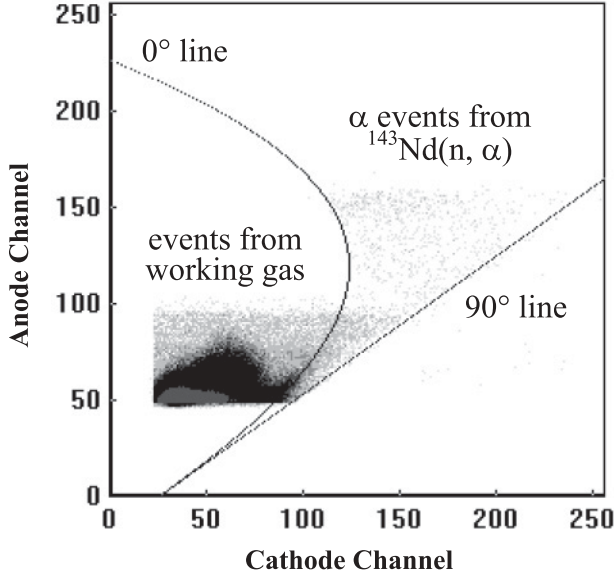
FIG. 2. Cathode-anode two-dimensional spectrum of forward events from the ^{143}Nd(n,α)^{140}Ce reaction at $E_n = 5.0$ MeV.

samples, respectively; and K is the neutron flux density ratio on ^{238}U and the measured samples.

K was calculated numerically using the diameters of samples and their distances to the gas target, length of the target, as well as the angular distributions of the ^{2}H(d,n)^{3}He reaction. For the ^{143}Nd(n,α)^{140}Ce reaction, the calculated values of K were 101.6, 96.7, and 92.5 for $E_n = 4.0, 5.0,$ and 6.0 MeV, respectively. For the ^{147}Sm(n,α)^{144}Nd reaction, the calculated values of K were 94.4 and 92.5 for 5.0 and 6.0 MeV, respectively. Relative uncertainty of K was 3%.

III. RESULTS AND DISCUSSION

Figure 2 shows the forward direction cathode-anode two-dimensional spectrum for the ^{143}Nd(n,α)^{140}Ce reaction measurement at $E_n = 5.0$ MeV. The area between the 0° and 90° lines [17] corresponds to the allowed region for α events from the ^{143}Nd(n,α)^{140}Ce reaction. At lower anode channels, background due to α events from the working gas obscures the signal of interest.

The anode spectrum projected for events between the 0° and 90° lines in Fig. 2 is shown in Fig. 3. Events from the ^{143}Nd(n,α)^{140}Ce reaction are clearly seen as a peak near channel 150. The counts in this peak above threshold (channel 110 in Fig. 3) $N_{\alpha_{\text{det}}}$ are less than the true number of counts N_α in formula (1) because, in addition to counts from ^{143}Nd(n,α)^{140}Ce or ^{147}Sm(n,α)^{144}Nd reactions that are below threshold, some α particles are absorbed by the target.

The relationship between N_α and $N_{\alpha_{\text{det}}}$ can be expressed as

$$N_\alpha = \frac{N_{\alpha\,\text{det}}}{1 - R}, \qquad (2)$$

where R is the ratio of α events below threshold (including absorbed ones) over total α events, which is much less than unity in the present work. Values of R depend on the α
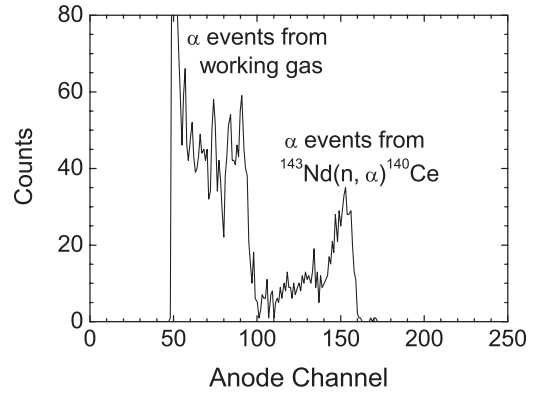
FIG. 3. Anode spectrum of forward events from the ^{143}Nd(n,α)^{140}Ce reaction at $E_n = 5.0$ MeV between the 0° and 90° lines.

threshold, α energy, and angular distribution, thickness, and material of the sample. R values were estimated for the two (n,α) reactions with different incident neutron energies and for forward and backward directions by Monte Carlo simulations of α straggling in the sample, using the measured forward/backward α counting ratio. In estimating R, α energies corresponding to transition to the ground state of the residual nuclei were used, because this component is expected to dominate the cross section because of Coulomb barrier effects. For the ^{143}Nd(n,α)^{140}Ce reaction, the estimated R value for forward α varied from 8.5% to 7.5% from $E_n = 4.0$ to 6.0 MeV, and that for backward α from 12% to 18%. For the ^{147}Sm(n,α)^{144}Nd reaction, R values at $E_n = 5.0$ MeV were 6.6% and 9.7% for forward and backward α, respectively; and at $E_n = 6.0$ MeV, 5.3% and 10.6%. The uncertainty of R was estimated to be about 25%. Sources of uncertainties of $N_{\alpha\,\text{det}}$ include statistics (2.4–5%) and background subtraction (3–5%). Therefore, the uncertainty of N_α is 5–8.5%.

Figure 4 shows the anode spectrum from the small ^{238}U fission chamber for $E_n = 5.0$ MeV, from which the number of fission counts N_f was obtained. The forward and backward cross sections were calculated using Eq. (1) and then added to get the total (n,α) cross section. The forward/backward cross section ratios depend only on the corrected numbers of forward and backward α events and the ratio of atom numbers in the
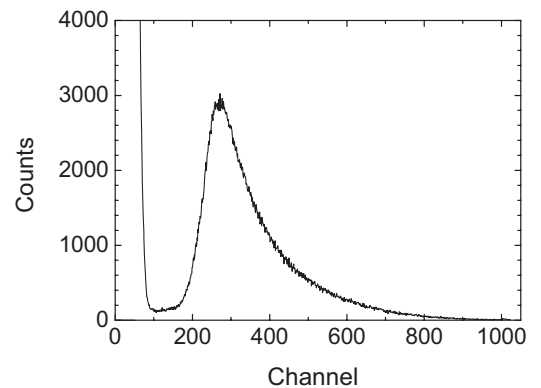
FIG. 4. Anode spectrum of the small ^{238}U fission chamber for the ^{143}Nd(n,α)^{140}Ce reaction measurement at $E_n = 5.0$ MeV.

TABLE II. Cross section data and forward/backward ratios in the laboratory reference system for the ^{143}Nd$(n,\alpha)^{140}$Ce reaction. Columns labeled "TALYS default" and "TALYS $0.5r_D$" were calculated with the default TALYS code parameter set and with α-optical model parameter r_D decreased to half of its default value, respectively.

E_n (MeV)	$\sigma_{n,\alpha}$ (mb)			Forward/backward ratio		
	Measured	TALYS default	TALYS $0.5r_D$	Measured	TALYS default	TALYS $0.5r_D$
4.0 ± 0.23	0.12 ± 0.012	0.289	0.120	1.25 ± 0.12	1.15	1.15
5.0 ± 0.16	0.21 ± 0.021	0.465	0.223	1.78 ± 0.18	1.33	1.35
6.0 ± 0.12	0.31 ± 0.031	0.899	0.502	2.50 ± 0.25	1.55	1.59

forward and backward samples. Hence, the uncertainties in these ratios are not affected by uncertainties of K, σ_f, N_f, and N_{238U} in Eq. (1). The final cross sections were corrected for attenuation of the neutron flux through the 2 mm thick aluminum wall of the ionization chamber and through the 2 mm thick aluminum backing of the two ^{147}Sm$_2$O$_3$ samples using the total neutron cross section of aluminum in ENFD/B-VII.0. Also, the small difference in average neutron energy in the measured and ^{238}U samples was taken into account when using the standard ^{238}U(n, f) cross sections from the ENDF/B-VII.0 library.

Cross sections and forward/backward ratios in the laboratory reference system for ^{143}Nd$(n,\alpha)^{140}$Ce and ^{147}Sm$(n,\alpha)^{144}$Nd reactions are given in Tables II and III. The main source of uncertainty in the cross sections is due to

uncertainties in the number of α events N_α (5–8.5%). Other sources of uncertainty include the neutron flux density ratio K (3%), fission counts N_f (2–2.5%), atom number in ^{143}Nd or ^{147}Sm (1.5%) and ^{238}U (1.3%) samples, and ^{238}U fission cross section (1%). The total relative uncertainty is about 10%.

Present cross sections for ^{143}Nd$(n,\alpha)^{140}$Ce and ^{147}Sm$(n,\alpha)^{144}$Nd reactions are compared with existing evaluations and experiments in Fig. 5. The cross section data near 14 MeV were obtained by integration of the differential cross section data of Augustyniak *et al.* [3,18] and Glowacka *et al.* [11]. One can see that there are very large differences between different evaluations, especially in the region of the
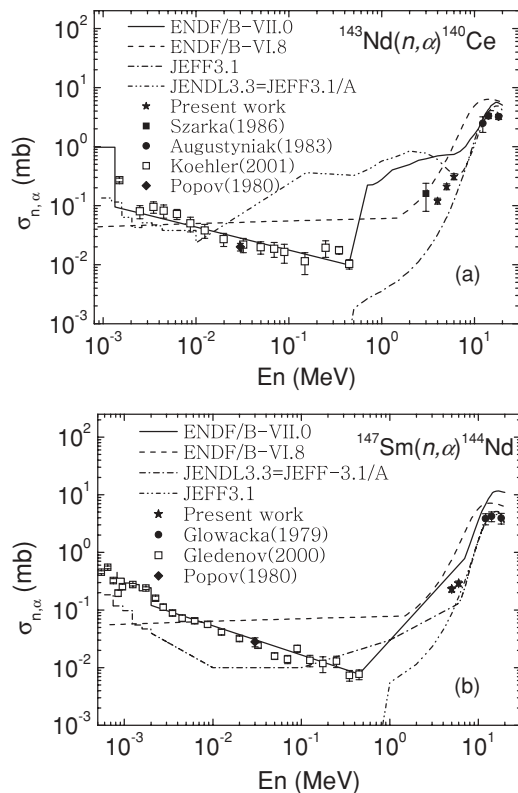
FIG. 5. Present cross sections compared with existing evaluations and measurements.
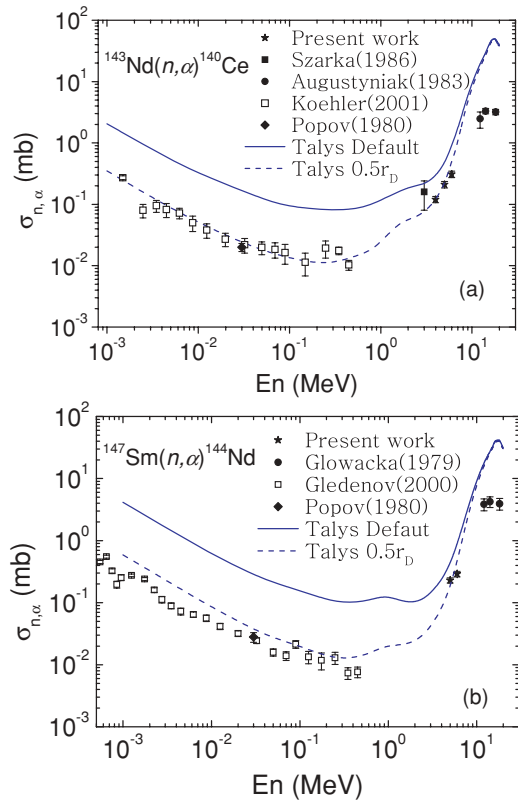
FIG. 6. (Color online) Present and previous cross sections compared with TALYS calculations. Calculations using default parameters as well as those made with α-optical potential parameter r_D reduced to half of its default value are shown as solid and dashed curves, respectively.

TABLE III. Same as Table II, but for the ^{147}Sm(n,α)^{144}Nd reaction.

E_n (MeV)	$\sigma_{n,\alpha}$ (mb)			Forward/backward ratio		
	Measured	TALYS default	TALYS $0.5r_D$	Measured	TALYS default	TALYS $0.5r_D$
5.0 ± 0.16	0.23 ± 0.023	0.438	0.185	1.65 ± 0.23	1.42	1.46
6.0 ± 0.12	0.29 ± 0.029	0.890	0.469	2.49 ± 0.32	1.62	1.68

present measurements, and that no evaluation is consistent with all the available data.

In an attempt to obtain better agreement with the data, the TALYS code [19] was used to calculate cross sections and forward/backward ratios. Results for the ^{143}Nd(n,α)^{140}Ce reaction are shown in Fig. 6(a) and Table II, and those for the ^{147}Sm(n,α)^{144}Nd reaction in Fig. 6(b) and Table III. Cross sections calculated using default TALYS parameters, as well as those using the available alternate α-optical potential, were, in general, substantially higher than the data. Conversely, calculated forward/backward ratios were consistently smaller than measured. Following the suggestion of Avrigeanu and Avrigeanu [20] that the diffuseness of the real part and surface imaginary well depth are most important, we adjusted parameters related to these parts of the α-optical potential. It was possible to obtain better agreement with the cross section data using several different adjustments of the available parameters. However, we could find no combination that would reproduce the data of Augustyniak *et al.* [3,18] and Glowacka *et al.* [11] near 14 MeV while still maintaining reasonable agreement with the other data. Also, parameter

changes leading to better agreement with the other cross section data resulted, in general, in similar forward/backward ratios. For example, the simplest means to obtain reasonably good agreement with all the data except those of 14 MeV was to adjust parameter r_D in TALYS to one-half its default value; results for this case are shown in Fig. 6 and Tables II and III.

These exploratory calculations indicate a considerable part of a direct component, and new measurements to check the results near 14 MeV as well as in the energy region between those data and the present results would be worthwhile.

[1] Yu. Andzheevski, V. K. Tkhan, V. A. Vtyurin, A. Koreivo, Yu. P. Popov, and M. Stempinski, Sov. J. Nucl. Phys. **32**, 774 (1980).

[2] Yu. Andzheevski, V. P. Vertebny, V. K. Tkhan, V. A. Vtyurin, A. L. Kirilyuk, and Yu. P. Popov, Yad. Phys. **48**, 20 (1988).

[3] W. Augustyniak, L. Glowacka, M. Jaskola, L. V. Khoi, J. Turkiewicz, and L. Zemlo, INDC(POL)-012, 7 (1983).

[4] E. Gadioli, E. GadioliErba, W. Augustyniak, L. Glowacka, M. Jaskola, J. Turkiewicz, and J. Dalmas, Phys. Rev. C **38**, 1649 (1988).

[5] P. E. Koehler, Yu. M. Gledenov, J. Andrzejewski, K. H. Guber, S. Raman, and T. Rauscher, Nucl. Phys. **A688**, 86 (2001).

[6] K. Okamoto, Nucl. Phys. **A141**, 193 (1970).

[7] Yu. P. Popov, V. I. Salackij, and G. Khuukhenkhuu, Sov. J. Nucl. Phys. **32**, 459 (1980).

[8] P. E. Koehler, Yu. M. Gledenov, T. Rauscher, and C. Frohlich, Phys. Rev. C **69**, 015803 (2004).

[9] Yu. M. Gledenov, P. E. Koehler, J. Andrzejewski, K. H. Guber, and T. Rauscher, Phys. Rev. C **62**, 042801(R) (2000).

[10] E. Gadioli, S. Mattioli, W. Augustyniak, L. Glowacka, M. Jaskola, J. Turkiewicz, and A. Chiadli, Phys. Rev. C **43**, 1932 (1991).

[11] L. Glowacka, M. Jaskola, J. Turkiewicz, and L. Zemlo, Nucl. Phys. **A329**, 215 (1979).

[12] N. P. Balabanov, Yu. M. Gledenov, P. H. Chol, Yu. P. Popov, and V. G. Semenov, Nucl. Phys. **A261**, 35 (1976).

[13] Yu. P. Popov, M. Przytula, R. F. Rumi, M. Stempinski, and M. Frontasyeva, Nucl. Phys. **A188**, 212 (1972).

[14] I. Szarka, M. Florek, and U. Jahn, Nucl. Instrum. Methods B **17**, 472 (1986).

[15] Evaluated Nuclear Data File, Database Version of January 16, 2009, url:http://www-nds.iaea.org/exfor/endf.htm.

[16] Guohui Zhang, Jiaguo Zhang, Li'an Guo, Hao Wu, Jinxiang Chen, Guoyou Tang, Yu. M. Gledenov, M. V. Sedysheva, G. Khuukhenkhuu, and P. J. Szalanski, Appl. Radiat. Isotopes **67**, 46 (2009).

[17] N. Ito, M. Baba, S. Matsuyama, I. Matsuyama, and N. Hirakawa, Nucl. Instrum. Methods A **337**, 474 (1994).

[18] EXFOR: Experimental Nuclear Reaction Data, Database Version of December 19, 2008, url:http://www-nds.iaea.org/exfor/exfor.htm. Accession # 30477002, 30477003, and 30477004.

[19] A. J. Koning, S. Hilaire, and M. C. Duijvestijn, in *Proceedings of the International Conference on Nuclear Data for Science and Technology–ND2007*, edited by O. Bersillon, F. Gunsing, E. Bauge, R. Jacqmin, and Sylvie Leray (EDP Sciences, Les Ulis, France, 2008), p. 211.

[20] M. Avrigeanu and V. Avrigeanu, Phys. Rev. C **79**, 027601 (2009).